Monoaryl derivatives as Transthyretin fibril formation inhibitors: design, synthesis, biological evaluation and structural analysis

Lidia Ciccone,[1,2] Susanna Nencetti,[1*] Nicolo Tonali,[3] Carole Fruchart-Gaillard,[4] William Shepard,[2] Elisa Nuti,[1] Caterina Camodeca,[1] Armando Rossello,[1,5] Elisabetta Orlandini [6,5*]

1. *Department of Pharmacy, University of Pisa, Via Bonanno 6, 56126, Pisa, Italy.*
2. *Synchrotron SOLEIL, L'Orme des Merisiers, Saint-Aubin, BP 48, 91192, Gif-sur-Yvette, France.*
3. *Université Paris-Saclay, CNRS, BioCIS, rue Jean-Baptiste Clément 5, 92290 Châtenay-Malabry, France*
4. *Université Paris Saclay, CEA, INRAE, Département Médicaments et Technologies pour la Santé (DMTS), SIMoS, 91191 Gif-sur-Yvette, France*
5. *Research Center "E. Piaggio", Università di Pisa, Pisa, 56122, Italy*
6. *Department of Earth Sciences, University of Pisa, Via Santa Maria 53-55, 56100, Pisa, Italy*

Abstract

Transthyretin (TTR) is a ß-sheet-rich homotetrameric protein that transports thyroxine (T4) and retinol both in plasma and in cerebrospinal fluid. TTR also interacts with amyloid-β, playing a protective role in Alzheimer's disease. Dissociation of the native transthyretin (TTR) tetramer is widely accepted as the critical step in TTR amyloids fibrillogenesis, and is responsible for extracellular deposition of amyloid fibrils. Small molecules, able to bind in T4 binding sites and stabilize the TTR tetramer, are interesting tools to treat and prevent systemic ATTR amyloidosis. We report here the synthesis, *in vitro* evaluation and three-dimensional crystallographic analyses of new monoaryl-derivatives in complex with TTR. Of the derivatives reported here, the best inhibitor of TTR fibrillogenesis, **1d**, exhibits an activity similar to diflunisal.

Keywords*: transthyretin, fibril formation inhibitors, X-ray TTR-ligand complexes, monoaryl*

Corresponding authors:

Dr. Susanna Nencetti, E-mail: susanna.nencetti@unipi.it

Prof. Elisabetta Orlandini, E-mail: elisabetta.orlandini@unipi.it

1. Introduction

Proteins misfolding and aggregating into various toxic aggregate structures are associated with many neurodegenerative diseases known as amyloid disorders. Transthyretin (TTR) is an amyloidogenic protein responsible for transthyretin-related amyloidosis (ATTR) caused by the deposition of fibrillar aggregates in extracellular tissue. ATTR is a systemic amyloidosis in which amyloid fibrils can be found in most organs thus interfering with their normal function.[1] The disease can exist in an autosomal dominant form, due to an inherited mutation in the TTR gene, or a non-hereditary form due to native TTR that is itself amyloidogenic. More than 120 single point mutations are described in the literature; the majority of these mutations increase the intrinsic amyloidogenic potential of TTR and are linked to TTR amyloid diseases such as familial amyloid polyneuropathy (FAP) and familial amyloid cardiomyopathy (FAC). Due to the loss of stability and function of the mutant TTR, amyloids deposit in the peripheral and autonomic nerves (FAP), or in the heart (FAC). Non-hereditary transthyretin amyloidosis (senile systemic amyloidosis; SSA), characterized by a late onset, is due to native TTR and affects about 20% of people over the age of 70, with a predominance in men.[2]

TTR is produced mainly by the liver and in minor amounts by retinal pigment epithelial cells and in the choroid plexus of the brain.[3][4][5] The main physiological function of TTR is the transport of thyroxine (T4) and retinol through the interaction with retinol-binding protein (RBP) in plasma, and of T4 in cerebrospinal fluid (CSF).[4] TTR also interacts with amyloid-β (Aβ) and plays a protective role in Alzheimer's disease (AD).[6][7][8] In AD patients, the level of several metals such as copper, iron and zinc drastically increases in neuritic plaque and amygdala.[9] The high metal concentrations acts as modulator of protein conformation,[10] and it has been reported that TTR in the presence of some metals, in particular Cu^{2+} and Fe^{2+}, undergoes a conformational change.[11][12] Moreover, an *in vitro* experiment has shown that in the presence of Cu^{2+} TTR-Aβ binding affinity increases from a micro- to nanomolar range, suggesting that Cu^{2+} has a relevant role as a Aβ scavenger.[12]

TTR is a 55 kDa homo-tetrameric protein composed of four identical subunits of 127 amino acid residues, β-sheet-rich, named A, A', B and B'. The four monomers are assembled according to a 222 symmetry to form two stable dimers (AB and A'B') associated back to back to generate the tetramer. At the dimer-dimer interface, the tetramer is crossed by a long channel coincident with one of the two-fold symmetric axes that defines two identical binding sites for the natural TTR ligand T4. Each site has a small inner and a larger outer binding subsite. The crystal complex between TTR and its natural ligand T4 shows three pairs of symmetric hydrophobic depressions,

which are occupied by the iodine atoms named halogen binding pockets (HBP1, HBP2, and HBP3).[13]

The wild-type TTR (wt-TTR) is potentially amyloidogenic because of its high degree of β-sheet structure. Biophysical studies demonstrated that wt-TTR is inclined to dissociation and through a multistep dynamic process fluctuates between the tetrameric structure and the folded monomeric form.[14][15] The intrinsic propensity towards β-aggregation, enhanced by amyloidogenic mutations, destabilizes the TTR tetramer and leads to its disassembly into folded monomers that easily unfold becoming amyloidogenic intermediates; these can spontaneously misassemble to form amyloid fibrils in the target tissue.[16] Dissociation of the TTR tetramer into its component subunits is the rate-limiting step in the amyloids formation process.[17] Under physiological conditions, only small amounts of T4 in the plasma is bound to TTR, the majority of TTR T4 binding sites are unoccupied (90-85%) and available to bind ligands to prevent tetramer dissociation.[18] Stabilization of the tetrameric state of TTR by small molecules binding to the TTR tetramer is a promising strategy to treat TTR amyloidosis. In fact, the binding of a small molecule into the T4-binding sites should stabilize the tetramer, slowing its conversion into monomers and amyloid fibrils. The first-in-class drug discovered with this strategy and directed to the treatment of FAP is Tafamidis meglumine (Vyndaqel ®)[19] that reached the European drug market in November 2011. Studies *in vitro*, *in vivo* and clinical trials for this drug confirmed that stabilization of the native tetrameric form of TTR is a promising approach to prevent or delay disease progression.[20][21]

The examination of the chemical structure of TTR amyloid inhibitors studied over the past decade [22], shows that the majority of TTR ligands discovered using structure-based design, possess the biaryl scaffold. To explore new and more simple chemical structures far from the typical halogenated biaryl scaffold of the non-steroidal anti-inflammatory drugs NSAID, we took into consideration a series of acid derivatives presenting only one aromatic portion.[23][24][25]

Our previous work reported the ability of some propionic acids of type **A** possessing a monoaryl structure to inhibit TTR fibril formation, see Figure 1.[23]

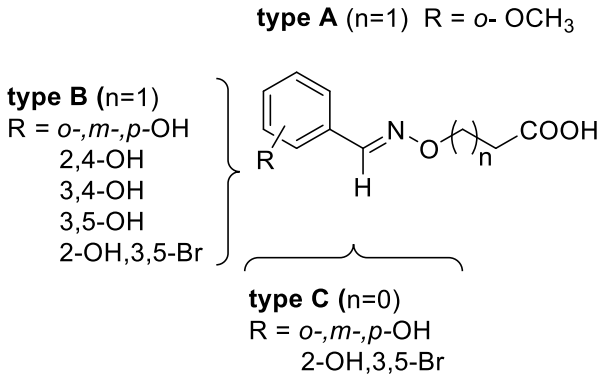

Figure 1. General formula of the previously reported mono-aryl compound (type **A**) and of the newly synthesized compounds (type **B** and **C**)

Among these, the compound in which R= *o*-OMe shows a good inhibition of TTR fibril formation. The crystal structure of this inhibitor bound to TTR (PDB 3GS7) shows that the carboxylic group of the inhibitor is placed in the outer binding pocket and oriented towards residues Lys15 and Lys15' while the *ortho*-methoxy substituent of the aromatic ring protrudes into halogen binding pockets 3 and 3'. This type of interaction is defined forward binding mode. The lead compound interacts with both T4 hormone binding pockets adopting two conformations with equal occupancy. [23]

The observation that many natural polyphenols such as curcumin, resveratrol, genistein and epigallocatechin gallate (EGCG) are able to stabilize the TTR tetramer [26][27][28][29][30], prompted us to functionalize the aromatic portion of mono aryl compounds of type **A** with mono- or di-hydroxyl groups in various positions of the aromatic ring or with a combination of hydroxyl group and halogen atoms to obtain new (aminoxy)propionic derivatives of type **B** (Figure 1). The (methylene)aminoxy (-CH=N-O-) linker and the carboxylic moiety that is essential for the interaction with keys amino acids in the T4 binding site (Lys15/15', Ser117/117', Thr119/119'), were both maintained.

Another modification of the chemical structure of type **A** compounds, was the reduction of the linker length of one carbon unit to obtain new hydroxyl-(aminoxy)acetic derivatives of type **C** (Figure 1). Our aim was to evaluate, the effect of a different linker length on the activity on the basis of the observation that in the monoaryl 9-fluorenyl-acetic derivative, previously studied by us (PDB 4TQH), the activity was maintained compared to the analogue propanoic one (PDB 4TQI)[24].

Therefore, in the present work new mono aryl compounds of type **B**, **1a-g** (Scheme 1) and of type **C**, **2a-d** (Scheme 2), were synthesized and their interaction with TTR was investigated using a turbidimetric UV assay. The ligands with a low percentage of fibril formation were also tested using

a Thioflavin T binding assay. Finally, to explain the biochemical results, we performed X-ray crystallographic analyses of the most active compounds in complex with TTR.

2. Chemistry

The (*E*) 3-(((mono-hydroxy- (**1a-c**), 3-(((3,5-dibromo-2-hydroxy- (**1d**), 3-(((di-hydroxy- (**1e-g**) benzylidene)amino)oxy)propanoic acids were prepared as shown in Scheme 1. Mitsunobu reaction between *N*-hydroxyphthalimide (**4**) and *tert*-butyl 3-hydroxypropanoate (**5**) yielded the *tert*-butyl 3-((1,3-dioxoisoindolin-2-yl)oxy)propanoate (**6**). Compound **6** after hydrolysis with 7M methanolic ammonia gave the 3-(aminooxy)propanoic acid that was crystallised as hydrochloride (**7**). Compound **7** was condensed with the opportune hydroxy aldehydes to obtain the (*E*)-3-((hydroxybenzylidene)amino)oxy)propanoic acid derivatives **1a-g**.

Scheme 1

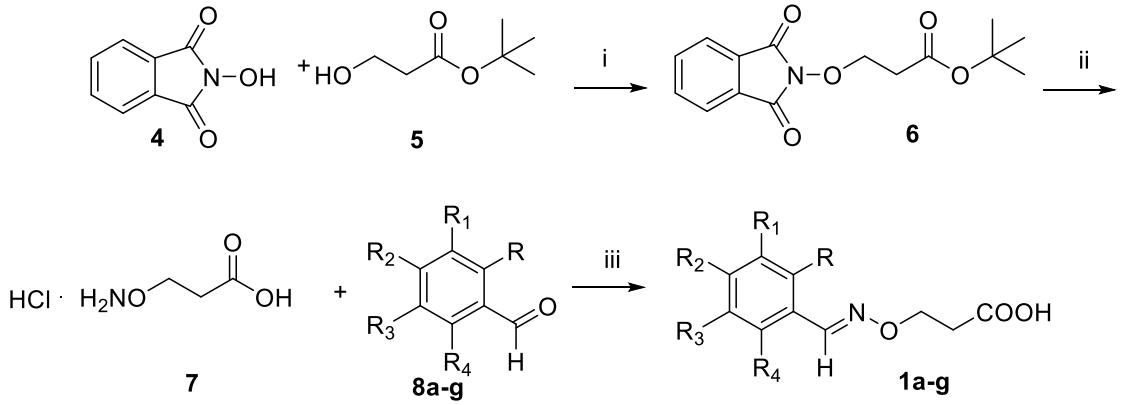

a, R=OH, R_1=R_2=R_3=R_4=H; **b**, R_1=OH, R=R_2=R_3=R_4=H; **c,** R_2=OH, R=R_1=R_3=R_4=H;**d,** R=OH, R_1=R_3=Br, R_2=R_4=H; **e,** R=R_2=OH, R_1=R_3=R_4=H; **f,** R1=R_2=OH, R=R_3=R_4=H; **g,** R_1=R_3=OH, R=R_1=R_3=H

Reaction conditions: **i,** P(Ph_3),DEAD,dryTHF,r.t. 72h; **ii**, NH_3/MeOH 7M, $CHCl_3$,r.t. 2h; **iii**, $CHCl_3$/H_2O, 40 °C.

Scheme 1. Synthesis of (amino)oxypropionic derivatives **1a-g**.

The (*E*)-2-((hydroxybenzylidene)amino)oxy)acetic acids (**2a-d**) and the (*E*)-2-(((carboxymethoxy)benzylidene)amino)oxy)acetic acid (**3i-n**) derivatives were prepared as described in Scheme 2. By reaction of the opportune hydroxyaldehyde **9a-d** with hydroxylamine hydrochloride the corresponding oximes **10a-d** of (*E*) configuration were obtained. The reaction of **10a-d** with ethyl 2-bromoacetate, yielded the corresponding desired mono esters **11a-d** or di-esters **12e-h** due to *O*-acylation. The esters **11a-d** and **12e-h** were hydrolysed using mild conditions with a

stoichiometric amount of 1M NaOH solution to yield the corresponding acids **2a-d** and **3i-n**, respectively. Dicarboxylic acids **3i-n**, obtained as products from the alkylation of phenolic groups with ethyl 2-bromoacetate, were also tested to assess their ability to inhibit TTR fibril formation.

Scheme 2

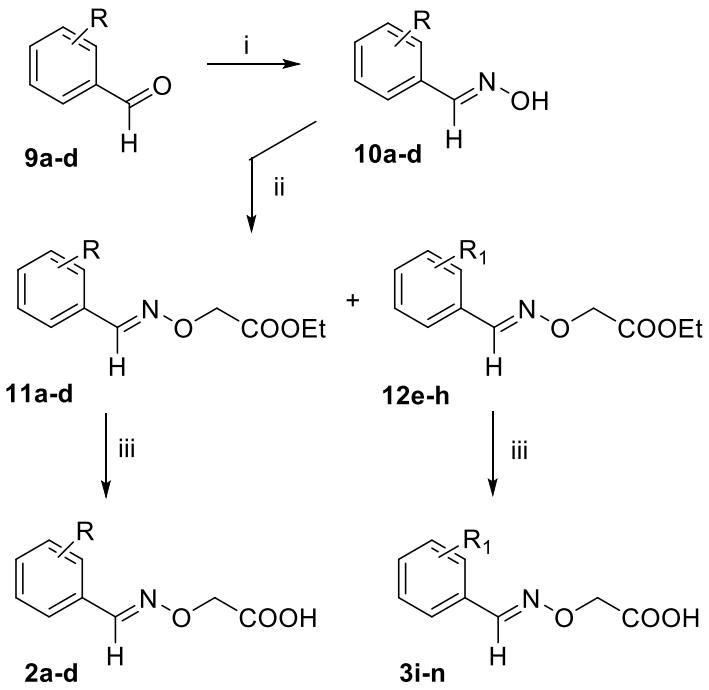

a, R=2-OH; **b,** R=3-OH; **c,** R=4-OH; **d**, R=2-OH,3,5-diBr; **e**, R_1= 2-OCH_2COOEt; **f**, R_1 3-OCH_2COOEt; **g**, R_1= 4-OCH_2COOEt; **h,** R_1= 2-OCH_2COOEt, 3,5-diBr-; **i**, R_1= 2-OCH_2COOH; **l**, R_1= 3-OCH_2COOH; **m**, R_1= 4-OCH_2COOH; **n**, R_1= 2-OCH_2COOH, 3,5-diBr-

Reaction conditions: **i,** $NH_2OH{\cdot}HCl$,DMSO/H_2O, r.t. 4h; **ii**, $BrCH_2COOEt$, CH_3CN, r.t. 3h; **iii**, NaOH,THF/H_2O, r.t. 3h;

Scheme 2. Synthesis of hydroxy aminoxyacetic derivatives **2a-d** and **3i-n**.

3. Results and discussion

3.1 Turbidimetric assay

The (*E*) 3-(mono-hydroxy)- (**1a-c**), or 3-(di-hydroxy)- (**1d-g**) ((benzylideneamino)oxy)propanoic acid derivatives and the (*E*)-2-((hydroxybenzylidene)amino)oxy)acetic acids (**2a-d)** and the (*E*)-2-(((carboxymethoxy)benzylidene)amino)oxy)acetic acids (**3i-n**) were tested *in vitro* against the amyloid fibril formation of TTR using the turbidimetric assay as previously described [24]. Results determined as a percentage of fibril formation are shown in Figure 2. The ability of the newly

synthesized compounds to reduce fibril formation was compared to diflunisal, used as reference drug (positive control), and TTR without inhibitor, used as the negative control. The inhibitor concentrations used in the turbidimetric assay was 7.2 μM, twice the TTR concentration in plasma (3.6 μM) and the values were acquired at 72 h.

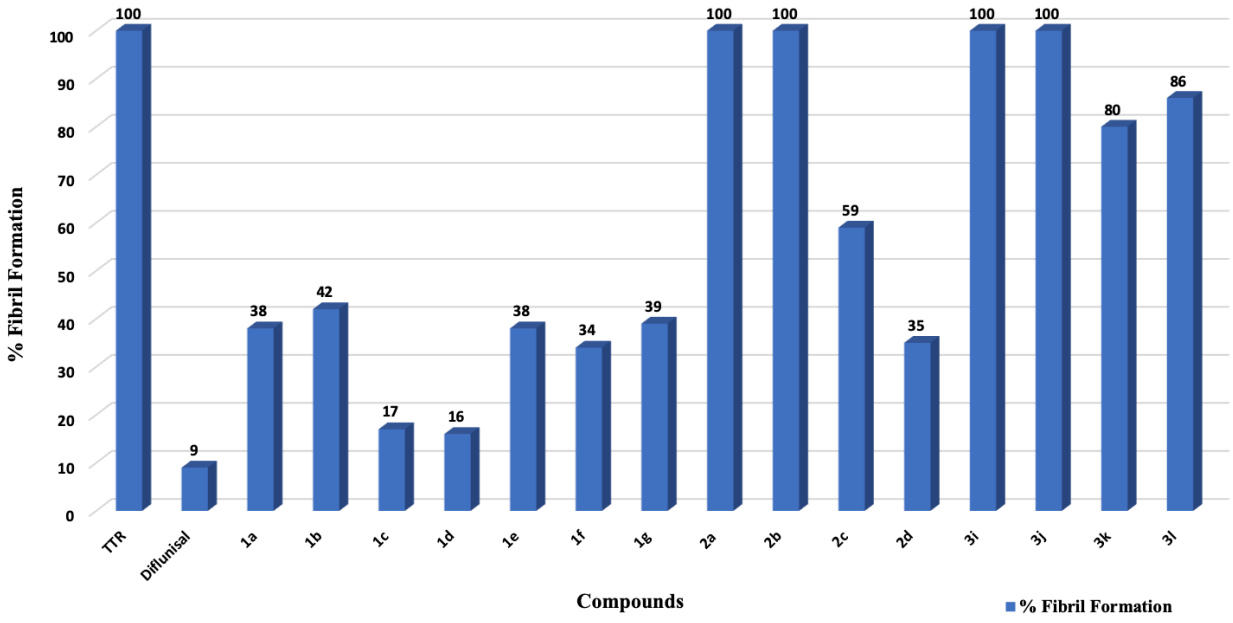

Figure 2. *In vitro* acid denaturation-mediated of WT-TTR. Bars represent data of type **B** and **C** compounds. The fibril formation in absence of inhibitor was assigned to be 100%. The error in the fibril formation assay is ±5%

An examination of the results obtained for the propanoic acids of type **B** that possess only one phenolic group (**1a-c**) shows that all compounds possess the ability to stabilize the TTR tetramer.
In particular, among the monohydroxy substituted compounds, the 4-OH-substituted derivative (**1c**) is the one that shows the best inhibitory effect on fibrillogenesis with a percentage of fibril formation of 17%. Instead, a hydroxyl group in 2 (**1a**) or 3 (**1b**) position of the aromatic ring decreases the inhibitory activity with a percentage of fibril formation of 38% and 42 %, respectively. An interesting result is obtained by the introduction of two bromine atoms in 3 and 5 position of the aromatic ring of the 2-OH substituted compound (**1a**). This modification leads to an increase of the ability to stabilize the TTR tetramer with a decrease in the of percentage of TTR fibril formation from 38 % with **1a** to 16% with the 3,5-dibromo-2-hydroxysubstitured derivative **1d**.

The inhibitory activity is moderately affected by the introduction of a second hydroxyl group: the catechol derivative (**1f**) presents a moderate ability to stabilize the TTR tetramer with 34% of fibril formation, while the 2,4-hydroxy (**1e**) and the 3,5-hydroxy substituted (**1g**) derivatives partially stabilize the TTR tetramer with 38% and 39% of fibril formation, respectively.

As regards to the ability of (*E*)-2-((hydroxybenzylidene)amino)oxy)acetic acid derivatives (**2a-d**) in inhibiting fibrillogenesis, only the 4–hydroxy substituted compound **2c** shows an inhibitory activity even if it is very moderate (59% fibril formation), while compounds **2a** and **2b** are devoid of any activity. As already seen for the aminoxy propanoic series, the formal introduction of a bromine atom at the 3 and 5 positions of the 2-hydroxy acetic acid derivative converts the inactive compound **2a** into a moderately active compound **2d** (35% of fibril formation).

The (carboxymethoxy)benzylidene)amino)oxy)acetic acids (**3i-n**) show a very low (**3m**, **3n**) or no ability to inhibit the TTR fibril formation (**3i**, **3l**).

These new monoaryl-acetic derivatives (**2a-d**), contrary to what has been highlighted by our previous study on monoaryl 9-fluorenyl-acetic derivative [24], efficient in stabilizing the tetramer, are less active than propanoic ones. We can hypothesize that this result is probably due to a weaker interaction in the active site of the TTR of the aryl portion with respect to the fluorenyl one that is able to occupy an alternative hydrophobic area in the TTR binding site. [23]

3.2 Thioflavin T binding assay

We speculated that our compounds could stabilize the tetramer structure and suppress amyloid fibril formation of wild-type TTR as could be observed by a Thioflavin T (ThT) binding assay. Starting from the turbidimetric result, we decided to further investigate the propanoic derivatives using the ThT binding assay. In particular, we selected the mono- ortho, meta and para substituted propanoic acid derivatives **1a-1c**, the 3,5-dibromo-2-hydroxysubstitured derivative **1d**, which showed the lowest percentage of fibril formation (16%), and among the di-substituted propanoic compounds **1e-g** (fibril formation ~ 34-39%), the derivative **1e**. Compound **1e** was chosen because, according to our reference lead compound (*o*-OCH_3, PDB 3GS7), it is substituted in ortho position, and in addition, the second hydroxyl group is located in the meta position as the second most active compound **1c** (fibril formation 17%). We incubated TTR samples with the indicated concentrations of inhibitors (10 μM) and EGCG, as a positive control, in acetate buffer (pH 4.4). We analysed them for amyloid fibril formation by registering the Thioflavin T fluorescence intensity at the end of the aggregation process (Figure 3). The presence of EGCG at 10 μM decreased the level of amyloidogenesis of wild-type TTR by at least 53% compared to the sample with TTR alone.[29] A slight decrease of the fluorescence was observed for compounds **1a** and **1b**, which can be considered less active than EGCG in the inhibition of TTR aggregation. Conversely, compounds **1c**

and **1d** showed a similar inhibitory activity to EGCG, with **1c** a little more active than **1d**. Surprisingly, compound **1e** resulted as the best inhibitor of the series, with an effect on the ThT fluorescence intensity decrease even better than EGCG (68% of inhibition and a significantly difference at $p < 0.001$, compared to the EGCG control). The slight discrepancy between the turbidimetric and ThT assay results for compound **1e** could be ascribed to the fact that ThT dye can recognize insoluble aggregates with high β-sheet content. It seems that in ThT assay compound **1e** is more active than observed in the turbidimetric test, probably because the ThT cannot bind to those aggregates which are responsible for the turbidity but not as well β-sheet structured to be detected by the fluorescent dye.

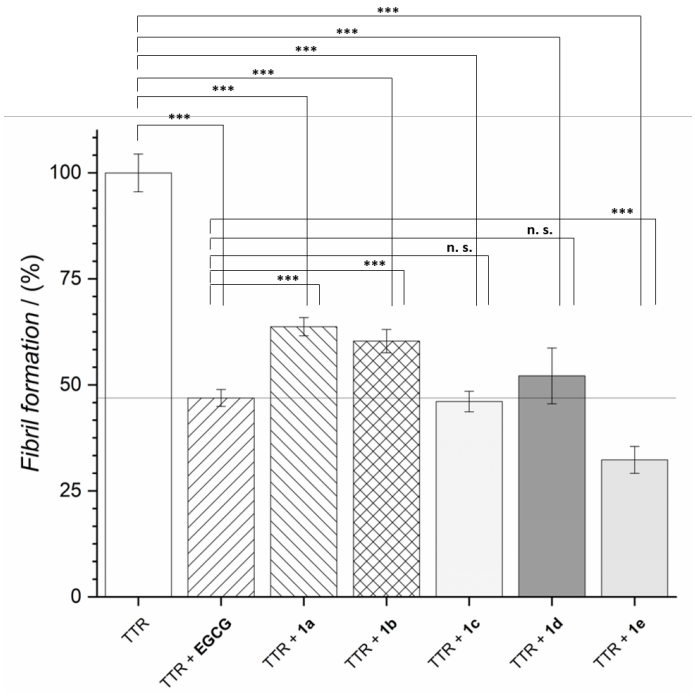

Figure 3. Percentage of TTR fibril formation assessed by ThT fluorescence assay (10 μM ThT in 50 mM glycine buffer; TTR final concentration at 0.045 μM). Amyloid fibril ratio (%) = 100 x (fluorescence TTR + compound / fluorescence without compound). Bars are representative of 11 measurements from the same experiment. Values represent the mean ± the standard error. Statistical significance was calculated by an ANOVA test (* $P < 0.05$, ** $P < 0.01$, *** $P < 0.001$, n.s. not significantly different).

3.3 Crystallographic Studies

In order to investigate the structure-activity relationships at an atomic level, crystal structures of the inhibitors **1c** (PDB 6TJN) and **1d** (PDB 6TI9) in complex with TTR have been obtained according to previously described procedures.[24][31] We selected these compounds because they show a

high percentage of fibril formation inhibition both in turbidimetric and in ThT assays, even if they are differently functionalized.

The crystals grown belong to the orthorhombic space group $P2_12_12$ with unit cell constants (Table 1) comparable to other TTR depositions in the PDB database. There are two monomers (A and B) in asymmetric unit, and by a two-fold crystallographic symmetry operation, monomer A and B form a tetramer (AB/A'B') in which the two T4-binging sites are located along the crystallographic 2-fold axis, see Figure 4.

In both crystal complexes, additional electron density is visible in both T4 binding pockets, confirming the presence of inhibitors **1c** and **1d**, respectively, see Figures 4 and 5. Ligands **1c** and **1d** bind along the two pockets with the same orientation: in forward mode, so that the carboxylic groups point towards Lys15 located at the entrance of the cavity, Figure 4. The occupancy of each ligand is fixed at 50% because they are located along the two-fold axis of the tetramer.

The two TTR monomers A and B display only minor differences between their protein structures. The root-main-square deviations (RMSD) calculated on C_α positions of the two crystal structures, 6TJN and 6TI9, is 0.38 Å, suggesting that there are no significant structural differences.

Structure	**TTR-1c**	**TTR-1d**
PDB code	**6TJN**	**6TI9**
Data Collection		
Source	SOLEIL Proxima2a	SOLEIL Proxima2a
Space group	*P*2$_1$2$_1$2	*P*2$_1$2$_1$2
Unit-cell		
a (Å)	43.32	43.14
b (Å)	85.99	85.82
c (Å)	64.09	63.84
Molec./asym.	2	2
Wavelength (Å)	0.980	0.919
Resolution (Å)	50-1.71	50-1.45
Highest resolution bin (Å)	1.72-1.71	1.46-1.45
No. of reflections	344252	569880
No. of unique reflections	26756	42800
Completeness (%)	99.8 (99.9)	99.9 (99.8)
I/σ (I)	22.90 (1.85)	16.29 (2.01)
$CC_{1/2}$	1.0 (0.74)	0.999 (0.75)
Rmerge (%)	6.0 (110)	8.1 (107.4)
Rp.i.m. (%)	5.8(105.5)	7.8(101.9)
Multiplicity	13.03 (12.68)	13.31 (10.02)
Refinement		
R-work	0.16 (0.174)	0.161 (0.155)
R-free	0.17 (0.192)	0.188 (0.182)
R.m.s. deviations		
Bond lengths (Å)	0.12	0.008
Bond angles (°)	1.3	0.95
Ramachandran		
Favored (%)	98.26	98.68
Outliers (#)	0	0

Table 1. Statistics for data collection, processing and refinement on TTR–ligand complexes.

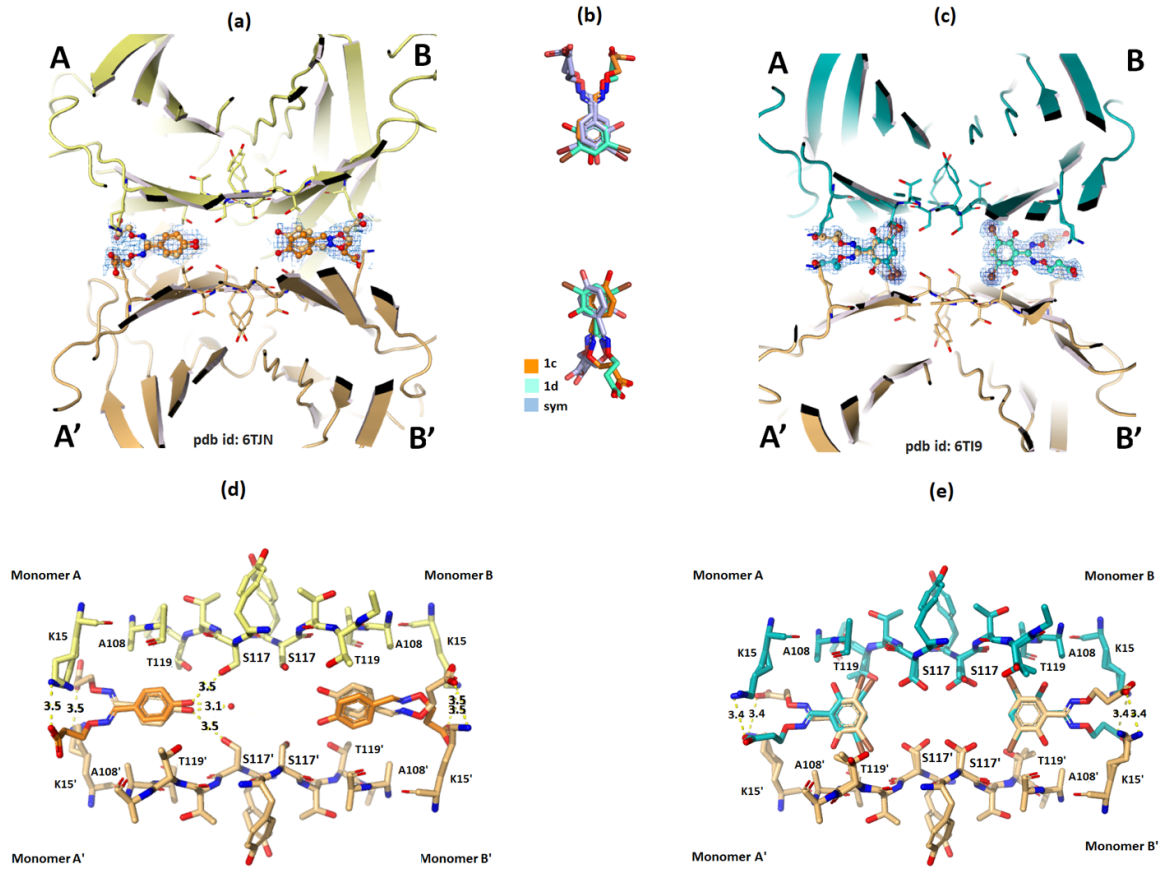

Figure 4. TTR-inhibitor crystal complexes: electron density and binding mode for propionic inhibitors **1c** and **1d**. (a) TTR tetramer in complex with compound **1c** (PDB 6TJN). The dimer formed by monomer A and B is represented in yellow, its symmetry light-orange. Ligand **1c** and its symmetric (orange and light orange respectively) bind both binding sites. Electron density (weighted 2Fo-Fc, contoured at 0.30, 0.8, 1.6, 2.5 σ) represented as multi-wire meshes. (b) Superposition of ligands **1c**, **1d** and their symmetric show minor differences in the accommodation of TTR binding sites. (c) Inhibitor **1d** in complex with TTR tetramer. Dimer A-B colored teal and the symmetry operation in light-orange. There is clear electron density (weighted 2Fo-Fc, contoured at 0.30, 0.8, 1.6, 2.5 σ) for ligand **1d** in both TTR binding sites. (d) Ligand **1c** binds in both TTR binding sites in forward mode. The binding modes are similar but not identical. H-bonds are showed with yellow dashes. (e) Ligand **1d** binds both T4 binding sites in forward mode.

The single crystal X-ray diffraction data of the TTR-**1c** crystal complex (6TJN) was collected to 1.7 Å resolution, the electron density map was shown in Figure 4 (a) and Figure S1. The phenolic moiety of compound **1c** is located in the inner cavities of both T4 binding sites. In the binding pocket A/A', the 4-hydroxyl group of the aromatic portion forms two hydrogen bonds, one with Ser117 (-OH – O Ser117 distance of 3.5 Å) and another with a water molecule (distance 3.1 Å), Figure 4 (d), while the carboxylic group of the propionic linker points towards Lys15/15' (COOH –

NH_2 of Lys15 distance 3.5 Å), see Figure 4 (a), (d). In the second binding pocket B/B', the polar interaction between the COOH and Lys 15 is preserved (COOH – NH_2 of Lys15 distance 3.5 Å), and a slight torsion of the aromatic portion orients the aromatic ring towards the hydrophobic pockets HBP3/HBP3', Figure 4 (a) (b) (d).

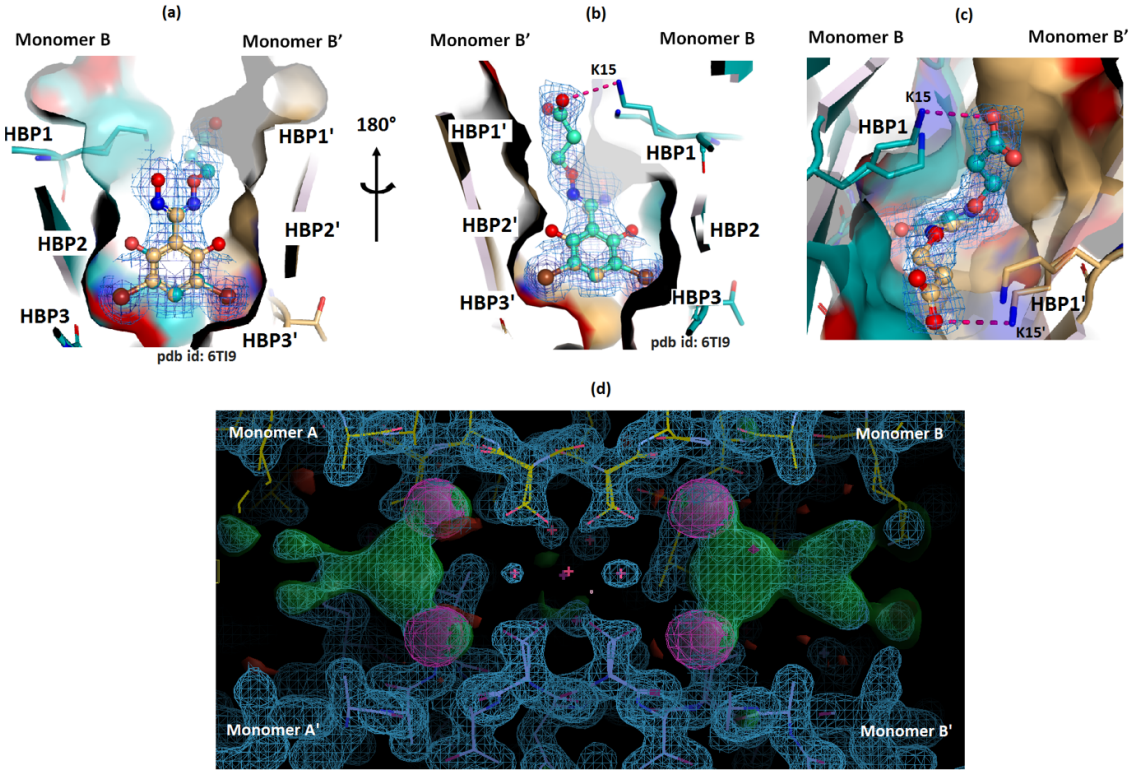

Figure 5. Electron density for the TTR-**1d** crystal complex. (a) Surface representation of the TTR tetramer shown with the ligand and its electron density sandwiched between two monomers (B-B'). The two bromine atoms are placed in HBP3 and HBP3'. (b) Ligand **1d** in complex with TTR. The figure was obtained rotating the dimer by 180° (B'-B). Red dashes show polar interaction between the carboxylic group and the Lys15. (c) View of the cavity B-B'. Hot-pink dashes display the interaction between the ligand and Lys15. (d) Experimental map shown in COOT for crystals grown in the presence of **1d**. The Fo-Fc Fourier map contoured at 3σ in green, 2Fo-Fc Fourier map is contoured at 1σ in blue mesh. Anomalous difference Fourier map of bromine atoms in purple contoured at 5σ.

The single crystal X-ray data for TTR in complex with (*E*)-3-(((3,5-dibromo-2-hydroxybenzylidene)amino)oxy)propanoic acid (**1d**) (6TI9) has been collected to 1.45 Å resolution (Table 1). Ligand **1d** binds to both T4 binding sites in forward mode, with the two bromine atoms placed into HBP3/HBP3' and the carboxylic moiety oriented towards Lys15/15' (COOH – NH_2 Lys15/Lys15' distance 3.4 Å) Figure 4 (b, c, e), and Figure 5 (a-d). To confirm the ligand binding mode, the data-set for TTR in complex with **1c** was collected just above the K absorption edge of bromine (0.919 Å) and a phased anomalous difference Fourier (DANO) map was calculated using

the refined model of TTR. Two high anomalous electron density peaks were identified in both of the inner T4 binding sites, HBP3 and HBP3'. This anomalous signal allows us to detect unambiguously the presence and the position of the two bromine atoms, Figure 5 (d).

The X-ray analysis of compounds **1c** and **1d** suggests that, for this type of monoaryl derivatives, the propionic linker has the correct length to strengthen the interaction between the -COOH moiety of the ligand and the -NH_2 group of Lys15 increasing the tetramer stabilization. Therefore, we can hypothesize that the acetic linker is not long enough to establish a strong and stable interaction between the ligand and binding pocket.

4. Conclusions

In the present work we have explored the effect produced by the decoration of a mono-aryl scaffold previously reported with hydroxyl and hydroxyl/halogen (Br) groups on the activity and the binding mode to TTR. The results of turbidimetric and thioflavin T binding assays presented here show that the (*E*)-3-((arylideneamino)oxy)propanoic acids (Type B, **1c** and **1d**) have the best activity with a percentage of inhibition of fibril formation values comparable to diflunisal and EGCG at the tested concentration. Moreover, this study shows that a single atom in the linker between the (arylideneamino)oxy and acidic moieties (Type C compounds) is not suitable to display any suitable inhibition of TTR fibril formation. The X-ray crystallographic studies have highlighted that for the propanoic acid derivatives of type B, both the halogen atoms (**1d**) and the 4-hydroxyl group (**1c**) drive the aromatic ring into the inner cavity, allowing the interaction of compounds in the *forward* binding mode. In the future, the decoration of mono-aryl moiety with a combination of groups, halogen/hydroxyl, in various positions, will be useful to better define the optimal fit of the propanoic acid derivatives in the T4 binding site.

Considering that transthyretin stabilization is a key point for the inhibition of transthyretin amyloidosis, the biological results and the structural data presented here identify the (arylidenamino)oxypropanoic acid structure as a promising scaffold for the design of effective TTR stabilizers.

5. Experimental

5.1. Material and methods

Analytical grade reagents and solvent were purchased from Sigma-Aldrich (St. Louis, MO), and were used as supplied. Solvents were dried according to standard methods. Melting points were determined on a Köfler hot-stage apparatus and are uncorrected. ^{1}H-NMR spectra of all synthesized

compounds were determined with a Bruker Ultrashield^{TM} 400 MHz (Fällander, Switzerland). Coupling constants *J* are reported in Hertz. The following abbreviations are used: singlet (s), doublet (d), doublet of doublet (dd), doublet of doublet of doublets (ddd), triplet (t), doublets of triplet (dt), broad (br) and multiplet (m). Reaction were monitored by thin layer chromatography (TLC) on silica gel plates containing a fluorescent indicator (Merck Silica Gel 60 F254), spots were detected under UV light (254 nm). Preparative TLC were performed with silica gel plates (2mm, Merck Silica Gel 60 F254). Chromatographic separations were performed on silica gel columns by flash column chromatography (Kieselgel 40, 0.040−0.063 mm; Merck). Na_2SO_4 was always used as the drying agent. Evaporation was carried out "in vacuo" (rotating evaporator). Elemental analyses were performed by our analytical laboratory and agreed with theoretical values to within ± 0.4%.

5.2. Synthetic procedure

*5.2.1. Tert-butyl 3-((1,3-dioxoisoindolin-2-yl)oxy)propanoate (**6**)*

To a stirred solution of 3-hydroxypropanoate (**5**) (1.71 mmol; 250 mg) and anhydrous THF (8.6 ml) were added under argon $P(Ph)_3$ (1.71 mmol; 448 mg), N-hydroxyphthalimide (**4**) (1.71 mmol; 279 mg) and DEAD (0.54 ml). The reaction mixture was stirred at room temperature for 72h then evaporated to dryness. The crude product was purified by flash chromatography on silica gel column, eluting with a mixture of EtOAc/hexane 1:9 to obtain **6** as on oil (230 mg, 46% yield); ^{1}H-NMR (400 MHz, $CDCl_3$) δ: 7.84-7.80 (m, 2H); 7.76-7.72 (m, 2H); 4.45 (t, 2H, *J*=6.8 Hz); 2.75 (t, 2H, *J*=6.8 Hz); 1.43 (s, 9H).

*5.2.2. 3-(aminooxy)propanoic acid hydrochloride (7•**HCl**)*

To a solution of **6** (0.789 mmol; 230 mg) in $CHCl_3$ (6.3 ml) was added ammonia in methanol solution (7M, 3.1 ml). The reaction mixture was stirred at room temperature (2h) until the disappearance of the starting compound (TLC, hexane/EtOAc 8:2). After evaporation to dryness the solid residue was dissolved in Et_2O and treated with an excess of Et_2O•HCl to yield a solid precipitate which was filtered and triturated with Et_2O to give pure **7•HCl** (38% yield). ^{1}H-NMR (400 MHz, CD_3OD-d_4) δ: 4.28 (t, 2H, *J*=5.8 Hz); 2.72 (t, 2H, *J*=5.8 Hz).

*5.2.3. General procedure for the synthesis of (E)-3-(((mono-hydroxy (**1a-c**), 2-hydroxy-3,5-bromo (**1d**) or di-hydroxy-(**1e-g**) benzylidene)amino)oxy)propanoic acids*

A stirred solution of the appropriate mono-hydroxy (**8a-c**), 2-hydroxy-3,5-dibromo- (**8d**) or di-hydroxy- (**8e-g**) benzaldehyde (0.96 mmol) in $CHCl_3$ (3 ml) was added 3-(aminooxy)propanoic acid hydrochloride (**7•HCl**) (1.06 mmol) in H_2O (1ml). The resulting mixture was stirred at 40°C until the disappearance of the starting compound (TLC, hexane/EtOAc 8:2) then diluted with H_2O and

extracted with $CHCl_3$. The chloroformic layer were washed (H_2O) dried and evaporated to dryness to yield the crude acids.

*(E)-3-(((2-hydroxybenzylidene)amino)oxy)propanoic acid (**1a**)*. The title compound was prepared from the aldehyde **8a** following the general procedure. The crude product was triturated with hexane to give the acid **1a** as white solid (56% yield); m.p. 114-116 °C; ^{1}H NMR (400 MHz, $CDCl_3$) δ: 9.59 (s, 1H, COOH); 8.19 (s, 1H, HC=N); 7.29 (t, 1H, *J*=7.2 Hz, Ar), 7.16 (d, 1H, *J*=7.2 Hz, Ar), 6.99 (d, 1H, *J*=8.0 Hz, Ar), 6.90 (t, 1H, *J*=7.2 Hz, Ar); 4.48 (t, 2H, *J*=6 Hz, OCH_2); 2.81 (t, 2H, *J*=6 Hz, CH_2CO);^{13}C NMR (400 MHz, $CDCl_3$) δ: 176.6 (C=O); 157.40 (C=N); 152.4 (1C, Ar-O); 131.5, 130.9, 119.7, 116.8, 116.1 (5 Ar-C); 69.6 (OCH_2); 34.1 (CH_2CO); Anal. Calcd for $C_{10}H_{11}NO_4$ (209.20); C, 57.41; H, 5.30; N, 6.70; Found 57.32; H, 5.39; N, 6.83.

*(E)-3-(((3-hydroxybenzylidene)amino)oxy)propanoic acid (**1b**)*. The title compound was prepared from the aldehyde **8c** following the general procedure. The crude product was purified by flash chromatography on silica gel column eluting with 2:1 n-hexane/EtOAc to give after trituration with hexane the acid **1b** as white solid (22 % yield); m.p. 107-109°C; ^{1}H NMR (400 MHz, DMSO-d_6) δ: 12.28 (s, 1H, COOH); 9.61 (s, 1H, OH); 8.14 (s, 1H, HC=N); 7.21 (t, 1H, *J*=7.2 Hz, Ar), 7.03-6.80 (m, 3H, Ar) ; 4.28 (t, 2H, *J*=6.4 Hz, OCH_2); 2.60 (t, 2H, *J*=6.4 Hz, CH_2CO). ^{13}C-NMR (400 MHz, DMSO-d_6) δ: 172.8 (C=O); 158.0 (C=N); 149.5 (1C, Ar-O); 133.5, 130.3, 118.7, 117.7, 113.4 (5 Ar-C); 69.9 (OCH_2); 34.5 (CH_2CO); Anal. Calcd for $C_{10}H_{11}NO_4$ (209.20); C, 57.41; H, 5.30; N, 6.70; Found 57.54; H, 5.38; N, 6.81.

*5.2.3.3 (E)-3-(((4-hydroxybenzylidene)amino)oxy)propanoic acid (**1c**)*. The title compound was prepared from the aldehyde **8c** following the general procedure. The crude product was purified by flash chromatography on silica gel column eluting with 3:1 n-hexane/EtOAc to give after trituration with hexane the acid **1c** as white solid (20% yield); m.p. 144-146 °C; ^{1}H NMR (400 MHz, CD_3OD-*d_4*) δ: 7.98 (s, 1H, HC=N); 7.42 (d, 2H, *J*=8.8 Hz, Ar); 6.76 (d, 2H, *J*=8.8 Hz, Ar); 4.35 (t, 2H, *J*=6.4 Hz, OCH_2). 2.64 (t, 2H, *J*=6.4 Hz, CH_2CO).^{13}C-NMR (400 MHz, CD_3OD-*d_4*) δ: 175.4 (C=O); 160.5 (C=N); 150.2 (1C, Ar-O); 129.7; 124.9; 116.5 (5 Ar); 70.4 (OCH_2); 35.4 (CH_2CO). Anal. Calcd for $C_{10}H_{11}NO_4$ (209.20); C, 57.41; H, 5.30; N, 6.70; Found 57.52; H, 5.25; N, 6.56.

*(E)-3-(((3,5-dibromo-2-hydroxybenzylidene)amino)oxy)propanoic acid (**1d**)*. The title compound was prepared from the aldehyde **8d** following the general procedure. The crude product was purified by flash chromatography on silica gel column eluting with (3:1 n-hexane/EtOAc) to give after trituration with hexane the acid **1d** as white solid (32%yield); m.p.: 129-130 °C; ^{1}H-NMR (400 MHz, $CDCl_3$) δ: 10.40 (s, 1H, COOH); 8.08 (s, 1H, HC=N); 7.66 (d, 1H, *J*=2.4 Hz, Ar); 7.24

(d, 1H, *J*=2.4 Hz, Ar); 4.50 (t, *J*=6 Hz, 2H, OCH_2); 2.80 (t, 2H, *J*=6 Hz, CH_2CO). ^{13}C-NMR (400 MHz, $CDCl_3$) δ: 175.3 (C=O); 153.3 (C=N); 150.4 (1C, Ar-O); 136.9, 132.4 (2C, Ar-Br); 118.5, 111.8, 111.4 (3C, Ar); 70.3 (OCH_2); 33.9 (CH_2CO). Anal. Calcd for $C_{10}H_9NO_4Br_2$ (366.98); C, 32.72; H, 2.45; N, 3.81; Found 32.71; H, 2.40; N, 3.81.

*(E)-3-(((2,4-dihydroxybenzylidene)amino)oxy)propanoic acid (**1e**)*. The title compound was prepared from the aldehyde **8e** following the general procedure. The crude product was triturated with hexane to give the acid **1e** as white solid **(**41% yield); m.p. 169-171 °C; ^{1}H-NMR (400 MHz, CD_3OD-*d_4*) δ: 8.17 (s, 1H, HN=C); 7.11 (d, 1H, *J*=8.4 Hz, Ar); 6.33 (ddd, 2H, *J*=10, 8, 1.6 Hz, Ar); 4.35 (t, 2H, *J*=6 Hz, OCH_2); 2.68 (t, 2H, *J*=6 Hz, CH_2CO); ^{13}C-NMR (400 MHz, CD_3OD-*d_4*) δ 175.1 (C=O); 161.9, 160.2 (2C Ar-O); 152.4 (C=N); 132.7, 110.3, 108.8, 103.7 (4C, Ar); 70.8 (OCH_2); 35.2 (CH_2CO). Anal. Calcd for $C_{10}H_{11}NO_5$ (225.19); C, 53.33; H, 4.92; N, 6.22; Found 53.42; H, 5.07; N, 6.34.

*(E)-3-(((3,4-dihydroxybenzylidene)amino)oxy)propanoic acid (**1f**)*. The title compound was prepared from the aldehyde **8f** following the general procedure. The crude product was triturated with hexane to yield the acid **1f** as white solid. (50% yield); m.p.: 163-165 °C; ^{1}H-NMR (400 MHz, DMSO-*d_6*) δ: 12.28 (s, 1H, COOH); 9.37 (s, 1H, OH); 9.18 (s, 1H, OH); 7.99 (s, 1H, HC=N); 7.05 (s, 1H, Ar), 6.84 (d, 1H, *J*=7.6 Hz, Ar); 6.73 (d, 1H, *J*=8.0 Hz, Ar); 4.23 (t, 2H, *J*=6 Hz, OCH_2); 2.59 (t, 2H, *J*=6 Hz, CH_2CO). ^{13}C-NMR (400 MHz, DMSO- *d_6*) δ: 172.9 (C=O); 149.5 (C=N); 148.1, 146.0 (2C, Ar-O); 123.6, 120.4, 116.0, 113.5 (4C, Ar); 69.6 (OCH_2); 34.5 (CH_2CO). Anal. Calcd for $C_{10}H_{11}NO_5$ (225.20); C, 53.33; H, 4.92; N, 6.22; Found 53.45; H, 5.03; N, 6.18.

*(E)-3-(((3,5-dihydroxybenzylidene)amino)oxy)propanoic acid (**1g**)*. The title compound was prepared from the aldehyde **8g** following the general procedure. The crude product was triturated with hexane to give the acid **1g** as white solid. (26% yield); m.p. 55-57°C; ^{1}H-NMR (400 MHz, MeOD-*d_4*) δ: 7.91 (s, 1H, HN=C); 6.52 (s, 2H, Ar); 6.28 (s, 1H, Ar); 4.36 (t, 2H, *J*=6 Hz, OCH_2); 2.68 (t, 2H, *J*=6 Hz, CH_2CO). ^{13}C-NMR (400 MHz, MeOD-*d_4*) δ: 175.2 (C=O); 159.9 (C=N); 150.5, 135.3 (2C, Ar-O); 106.6, 105.3 (2C, Ar); 70.6 (OCH_2); 35.3 (CH_2CO). Anal. Calcd for $C_{10}H_{11}NO_5$ (225.20); C, 53.33; H, 4.92; N, 6.22; Found 53.26; H, 4.80; N, 6.11.

*5.2.4. General procedure for the synthesis of (E)-hydroxybenzaldehyde oximes (**10a-d**)*

To a solution of the opportune hydroxybenzaldehyde **9a-d** (4.1 mmol) in DMSO (3 ml) was added an aqueous (2 ml) solution of NH_2·HCl (14.3 mmol). The reaction mixture was stirred at room

temperature for 4h then diluted with H_2O and extracted with EtOAc and the organic extracts washed with H_2O. The evaporation of the dried organic layer gave a solid residue that was triturated with $CHCl_3$ and the product was filtered and purified crystallization (Et_2O/Hex) to obtain **10a-d** pure.

*(E)-2-hydroxybenzaldehyde oxime (**10a**)*: (87% yield); m.p. 56-58°C; ^{1}H-NMR (400 MHz, DMSO-d_6) δ: 11.30 (s, 1H, OH-Ar). 10.07 (s, 1H, HON=C), 8.33 (s, 1H, HC=N), 7.50 (dd, 1H, *J*=7.68, *J*=1.60 Hz, Ar), 7.22 (ddd, 1H, *J*=8.3, 7.2, 1.6 Hz, Ar), 6.98-6.83 (m, 2H, Ar).

*(E)-3-hydroxybenzaldehyde oxime (**10b**)*: (40% yield); m.p. 85-87 °C; ^{1}H-NMR (400 MHz, DMSO-d_6) δ: 11.09 (s, 1H, OH); 9.47 (s, 1H, HON=C), 7.97 (s, 1H, HC=N); 7.12 (t, 1H, *J*=7.6 Hz, Ar); 6.95 (dd, 1H, *J*=4.0, 1.6 Hz, Ar), 6.91 (d, 1H, *J*=7.6 Hz, Ar); 6.00 (ddd, 1H, *J*=8.4, 2.8, 1.2 Hz, Ar).

*(E)-4-hydroxybenzaldehyde oxime (**10c**)*: (66% yield); m.p. 92-94°C; ^{1}H-NMR (400 MHz, DMSO-d_6) δ: 10.82 (s, 1H, OH). 9.74 (s, 1H, HON=C); 7.99 (s, 1H, HC=N); 7.40 (d, 2H, *J*=8.8 Hz, Ar), 6.77 (d, 2H, *J*=8.8 Hz, Ar).

*(E)-3,5-dibromo-2-hydroxybenzaldehyde oxime (**10d**)*: (95% yield); m.p. 208-210 °C; ^{1}H-NMR (400 MHz, DMSO-d_6) δ: 11.92 (s, 1H, OH-Ar), 10.97 (s, 1H, OHN=C), 8.35 (s, 1H, CH=N), 7.74 (s, 1H, Ar), 7.67 (s, 1H, Ar).

*5.2.5. General procedure for the synthesis of ethyl (E)-2-(((hydroxybenzylidene)amino)oxy)acetate derivatives (**11a-d**) and ethyl (E)-2-(((2-ethoxy-2-oxoethoxy)benzylideneamino)oxy)acetate derivatives (**12e-h**)*

To a solution of hydroxybenzaldoxime (3.66 mmol) in CH_3CN (3 ml) and ethyl bromoacetate (3.66 mmol) were added Cs_2CO_3 (3.66 mmol). The reaction mixture was stirred at room temperature for 3h until the disappearance of the starting compound (TLC, hexane/EtOAc 8:2). After filtration of the excess Cs_2CO_3 the reaction mixture was added with AcOEt, washed several times with H_2O, dried with Na_2SO_4 and finally evaporated at reduced pressure to obtain a crude solid. The crude product was constituted by two products that were separated by FLASH chromatography on silica-gel eluting with 3:1 AcOEt/hexane. From the collected evaporated fractions two compounds were obtained as white solids which were crystallized from a mixture of Et_2O/hexane to give the monoesters **11a-d** and diesters **12e-h.**

*Ethyl (E)-2-(((2-hydroxybenzylidene)amino)oxy)acetate (**11a**)*: (17% yield); ^{1}H-NMR (400 MHz, $CDCl_3$) *δ*: 9.43 (s, 1H, OH); 8.31 (s, 1H, HC=N); 7.30 (ddd, 1H, *J*=8.4, 7.2, 1.6 Hz Ar); 7.18 (dd,

1H, *J*=7.6, 1.6, Hz Ar); 6.97 (dd, 1H, *J*=7.6, 1.6 Hz Ar); 6.92 (dd, 1H, *J*=7.6, 1.2 Hz Ar); 4.70 (s, 2H, OCH_2), 4.26 (q, 2H, *J*=7.1 Hz, $COCH_2$); 1.30 (t, 3H, *J*=7.1 Hz, CH_3).

*Ethyl (E)-2-(((3-hydroxybenzylidene)amino)oxy)acetate (**11b**)*: (40% yield); ^{1}H-NMR (400 MHz, DMSO-d_6) δ: 11.26 (s, 1H, OH); 8.08 (s, 1H, HC=N); 7.28 (t, 1H, *J*=8.0 Hz, Ar); 7.19 (d, 1H, *J*=7.6 Hz, Ar); 7.12 (dd, 1H, *J*=2.4, 1.2 Hz, Ar); 6.92 (ddd, 1H, *J*=8.2, 2.4, 0.8 Hz, Ar); 4.78 (s, 2H, OCH_2), 4.15 (q, 2H, *J*=7.0 Hz, $COCH_2$); 1.19 (t, 3H, *J*=7.0 Hz, CH_3).

*Ethyl (E)-2-(((4-hydroxybenzylidene)amino)oxy)acetate (**11c**)*: (15% yield); ^{1}H-NMR (400 MHz, $CDCl_3$) *δ*: 11.00 (s, 1H, OH); 8.06 (s, 1H, HC=N); 7.51 (d, 2H, *J*=8.8 Hz, Ar); 6.94 (d, 2H, *J*=8.8 Hz, Ar); 4.80 (s, 2H, OCH_2), 4.16 (q, 2H, *J*=7.0 Hz, $COCH_2$); 1.21 (t, 3H, *J*=7.0 Hz, CH_3).

*Ethyl (E)-2-(((3,5-dibromo-2-hydroxybenzylidene)amino)oxy)acetate (**11d**)*: 52% yield); ^{1}H-NMR (400 MHz, DMSO-d_6) δ: 10.31 (s, 1H, OH); 8.53 (s, 1H, HC=N); 7.85 (d, 2H, *J*=2.4 Hz, Ar); 7.68 (d, 2H, *J*=2.4 Hz, Ar); 4.85 (s, 2H, OCH_2), 4.16 (q, 2H, *J*=7.0 Hz, $COCH_2$); 1.21 (t, 3H, *J*=7.0 Hz, CH_3).

*Ethyl (E)-2-(((3-(2-ethoxy-2-oxoethoxy)benzylidene)amino)oxy)acetate (**12e**)*: (51% yield); ^{1}H-NMR (400 MHz, $CDCl_3$) δ: 8.67 (s, 1H, HC=N); 7.78 (dd, 1H, *J*=7.7, 1.7 Hz, Ar); 7.18 (dd, 1H, *J*=7.6, 1.6 Hz, Ar); 7.31 (ddd, 1H, *J*=8.4, 7.2, 1.6 Hz, Ar); 6.97 (t, 1H, *J*=7.6 Hz, Ar); 6.76 (d, 1H, *J*=7.6 Hz, Ar); 4.69 (s, 2H, OCH_2), 4.64 (s, 2H, OCH_2), 4.25 (q, 2H, *J*=7.2 Hz, $COCH_2$); 4.24 (q, 2H, *J*=7.2 Hz, $COCH_2$); 1.29 (t, 3H, *J*=7.2 Hz, CH_3); 1.29 (t, 3H, *J*=7.2 Hz, CH_3).

*Ethyl (E)-2-(((3-(2-ethoxy-2-oxoethoxy)benzylidene)amino)oxy)acetate (**12f**)*: (28% yield); ^{1}H-NMR (400 MHz, DMSO-d_6) *δ*: 8.32 (s, 1H, HC=N); 7.36 (t, 1H, *J*=8.0 Hz, Ar); 7.21 (d, 1H, *J*=7.6 Hz, Ar); 7.14 (dd, 1H, *J*=2.5, 1.4 Hz, Ar); 7.00 (ddd, 1H, *J*=8.2, 2.4, 0.8 Hz, Ar); 4.79 (s, 2H, OCH_2), 4.73 (s, 2H, OCH_2), 4.15 (q, 4H, *J*=7.0 Hz, $COCH_2$); 1.20 (t, 6H, *J*=7.0 Hz, CH_3).

*Ethyl (E)-2-(((4-(2-ethoxy-2-oxoethoxy)benzylidene)amino)oxy)acetate (**12g**)*: (10% yield); ^{1}H-NMR (400 MHz, DMSO-d_6) *δ*: 8.24 (s, 1H, HC=N); 7.54 (d, 2H, *J*=8.8 Hz, Ar); 6.98 (d, 2H, *J*=8.8 Hz, Ar); 4.82 (s, 2H, OCH_2), 4.69 (s, 2H, OCH_2), 4.14 (q, 2H, *J*=7.2 Hz, $COCH_2$); 4.13 (q, 4H, *J*=7.2 Hz, $COCH_2$);1.20 (t, 3H, *J*=7.2 Hz, CH_3); 1.18 (t, 3H, *J*=7.2 Hz, CH_3).

*Ethyl (E)-2-(((3,5-dibromo-2-(2-ethoxy-2-oxoethoxy)benzylidene)amino)oxy)acetate (**12h**):* (21% yield); ^{1}H-NMR (400 MHz, DMSO-d_6) δ: 8.61 (s, 1H, HC=N); 8.00 (d, 2H, *J*=2.4 Hz, Ar); 7.77 (d, 2H, *J*=2.4 Hz, Ar); 4.97 (s, 2H, OCH_2), 4.73 (s, 2H, OCH_2); 4.18 (q, 2H, *J*=7.1 Hz, $COCH_2$); 4.15 (q, 2H, *J*=7.1 Hz, $COCH_2$); 1.22 (t, 3H, *J*=7.1 Hz, CH_3); 1.21 (t, 3H, *J*=7.1 Hz, CH_3).

*5.2.6. General procedure for the synthesis of (E)-2-(((hydroxybenzylidene)amino)oxy)acetic acids (**2a-d**) and (E)-2-(((2-ethoxy-2-oxoethoxy)benzylideneamino)oxy)acetic acids (**3i-n**).*

To a solution of the appropriate ethyl ester **11a-d** and **12 e-h** (1.10 mmol) in 9 ml of H_2O and 18 ml of THF was added a solution of NaOH 1N (2.20 ml). The reaction mixture was stirred at r.t. for about 3h monitoring by TLC. After evaporation of THF, the aqueous phase was washed with EtOAc cooled at 0 °C and acidified with 1N HCl to pH = 3, then extracted with EtOAc and the organic extracts washed with H_2O. The evaporation of the organic layer gave a crude solid which was purified by crystallization from a mixture of Et_2O/hexane providing the desired acids ***2a-d*** and ***3i-n*** as a white crystalline solid.

*(E)-2-(((2-hydroxybenzylidene)amino)oxy)acetic acid (**2a**)*: (70% yield); m.p.: 162-163 °C; ^{1}H-NMR (400 MHz CD_3OD-d_4) δ: 8.42 (s, 1H, HC=N); 7.39 (dd, 1H, *J*=8.0, 1.6 Hz, Ar); 7.26 (dt, 1H, *J*=8.0, 1.6 Hz, Ar); 6.89-6.86 (m, 2H, Ar); 4.70 (s, 2H, OCH_2). ^{13}C-NMR (400 MHz, CD_3OD-d_4) δ: 173.3 (C=O); 158.2 (C=N); 152.3 (C, Ar-O); 132.6, 130.9, 120.7, 118.0, 117.3 (5C, Ar); 71.6 (OCH_2). Anal. Calcd for $C_9H_9NO_4$ (195.17); C, 55.38; H, 4.64; N, 7.17; Found 55.35; H, 4.60; N, 7.16.

*(E)-2-(((3-hydroxybenzylidene)amino)oxy)acetic acid (**2b**)*: (77% yield); m.p.: 108-109°C; ^{1}H-NMR (400 MHz, CD_3OD-d_4) δ: 8.04 (s, 1H, HC=N); 7.28 (t, 1H, *J*=7.8 Hz, Ar); 7.18 (dd, 1H, *J*=6.1, 2.5 Hz, Ar); 6.64 (ddd, 1H, *J*=8.2, 2.6, 0.92 Hz, Ar); 4.91 (s, 2H, OCH_2). ^{13}C-NMR (400 MHz, CD_3OD-d_4) δ: 172.5 (C=O); 159.7 (C=N); 149.8 (C, Ar-O); 135.9, 130.8, 121.4, 117.1, 113.0 (5C, Ar); 65.8 (OCH_2). Anal. Calcd for $C_9H_9NO_4$ (195.17); C, 55.38; H, 4.64; N, 7.17; Found 55.34; H, 4.61; N, 7.17.

*(E)-2-(((4-hydroxybenzylidene)amino)oxy)acetic acid (**2c**)*: (80% yield); m.p.: 157-158°C; ^{1}H-NMR (400 MHz, CD_3OD-d_4) δ: 8.02 (s, 1H, HC=N); 7.52 (d, 2H, *J*=8.5 Hz, Ar); 6.93 (d, 2H, *J*=8.5 Hz, Ar); 4.68 (s, 2H, OCH_2). ^{13}C-NMR (400 MHz, CD_3OD-d_4) δ: 172.4 (C=O); 160.5 (C=N); 149.7 (C, Ar-O); 129.2, 127.8, 115.8 (5C, Ar); 65.8 (OCH_2). Anal. Calcd for $C_9H_9NO_4$ (195.17); C, 55.38; H, 4.64; N, 7.17; Found 55.36; H, 4.63; N, 7.15.

*(E)-2-(((3,5-dibromo-2-hydroxybenzylidene)amino)oxy)acetic acid (**2d**)*: (70% yield); m.p.: 178-180°C; ^{1}H-NMR (400 MHz, CD_3OD-d_4) δ: 8.40 (s, 1H, HC=N); 7.71 (d, 1H, *J*=2.4 Hz, Ar); 7.57 (d, 1H, *J*=2.4 Hz, Ar); 4.75 (s, 2H, OCH_2). ^{13}C-NMR (400 MHz, CD_3OD-d_4) δ: 173.3 (C=O); 154.4 (C=N); 151.2 (C, Ar-O); 137.8, 133.1 (2C, Ar-Br); 121.2, 112.8, 112.6 (3C, Ar); 72.3 (OCH_2). Anal. Calcd for $C_{10}H_9NO_4Br_2$ (354.97); C, 30.40; H, 2.55; N, 3.94; Found 30.39; H, 2.48; N, 3.90.

*(E)-2-(((2-(carboxymethoxy)benzylidene)amino)oxy)acetic acid (**3i**)*: (72% yield); m.p.: 187-188°C; ^{1}H-NMR (400 MHz, CD_3OD-d_4) δ: 8.63 (s, 1H, HC=N); 7.74 (dd, 1H, *J*=7.6, 1.6 Hz, Ar); 7.35 (dt,

1H, *J*=7.4, 1.6 Hz, Ar); 6.97 (t, 1H, *J*=7.0 Hz, Ar); 6.94 (d, 1H, *J*=8.4 Hz, Ar); 4.74 (s, 2H, OCH_2); 4.68 (s, 2H, OCH_2). ^{13}C-NMR (400 MHz, CD_3OD-d_4) δ: 173.5, 171.9 (2C, C=O); 157.4 (C=N); 147.0 (C, Ar-O); 132.4, 127.3, 122.4, 121.8, 113.4 (5C, Ar); 71.2, 66.1 (2C, OCH_2). Anal. Calcd for $C_{11}H_{11}NO_6$ 253.20); C, 52.17; H, 4.37; N, 5.53; Found 52.10; H, 4.30; N, 5.46.

*(E)-2-(((3-(carboxymethoxy)benzylidene)amino)oxy)acetic acid (**3l**):* (75% yield); m.p.: 144-145°C; ^{1}H-NMR (400 MHz, CD_3OD-d_4) δ: 8.18 (s, 1H, HC=N); 7.31 (t, 1H, *J*=8.0 Hz, Ar); 7.21 (dd, 1H, *J*=5.7, 1.8 Hz, Ar); 7.00 (dd, 1H, *J*=2.6, 1.0 Hz, Ar); 6.98 (t, 1H, *J*=1.84 Hz, Ar); 4.69 (s, 2H, OCH_2); 4.68 (s, 2H, OCH_2). ^{13}C-NMR (400 MHz, CD_3OD-d_4) δ: 172.4, 171.2 (2C, C=O); 158.5 (C=N); 150.0 (C, Ar-O); 133.4, 129.7, 120.6, 116.7, 112.3 (5C, Ar); 70.2, 64.6 (2C, OCH_2). Anal. Calcd for $C_{11}H_{11}NO_6$ (253.20); C, 52.17; H, 4.37; N, 5.53; Found 52.11; H, 4.32; N, 5.50.

*(E)-2-(((4-(carboxymethoxy)benzylidene)amino)oxy)acetic acid (**3m**)*: (72% yield); m.p.: 176-177°C; ^{1}H-NMR (400 MHz, CD_3OD-d_4) δ: 8.14 (s, 1H, HC=N); 7.55 (d, 2H, *J*=8.8 Hz, Ar); 6.95 (d, 2H, *J*=8.8 Hz, Ar); 4.69 (s, 2H, OCH_2); 4.65 (s, 2H, OCH_2). ^{13}C-NMR (400 MHz, CD_3OD-d_4) δ: 173.8, 171.3 (2C, C=O); 161.1 (C=N); 150.9 (C, Ar-O); 127.8, 126.5, 115.9 (5C, Ar); 71.4, 65.8 (2C, OCH_2). Anal. Calcd for $C_{11}H_{11}NO_6$ (253.20); C, 52.17; H, 4.37; N, 5.53; Found 52.10; H, 4.31; N, 5.49.

(E)-2-(((3,5-dibromo-2-(carboxymethoxy)benzylidene)amino)oxy)acetic acid (***3n***): (68% yield); m.p.: 214-216 °C; ^{1}H-NMR (400 MHz CD_3OD-d_4): 8.59 (s, 1H, HC=N); 7.88 (d, 1H, *J*=2.4 Hz, Ar); 7.82 (d, 1H, *J*=2.4 Hz, Ar); 4.72 (s, 2H, OCH_2), 4.62 (s, 2H, OCH_2). ^{13}C-NMR (400 MHz, CD_3OD-d_4): 173.6, 171.7 (2C, C=O); 154.4 (C=N); 145.9 (C, Ar-O); 138.1, 130.3, (2C, Ar-Br); 129.8, 119.2, 119.0 (3C, Ar); 71.8, 71.3 (2C, OCH_2). Anal. Calcd for $C_{10}H_9NO_4Br_2$ (410.99); C, 32.16; H, 2.20; N, 3.40; Found 32.00; H, 2.00; N, 3.20.

5.3 Turbidimetric assay

The percentage of fibril formation was determined following a procedure previously described [23] by observing the turbidity of wild-type TTR at pH = 4.4 in the presence and in the absence of an inhibitor. Commercially available Prealbumin, Human Plasma (wt-TTR) was purchased from Calbiochem (EDM Millipore). In brief, the compounds under study and diflunisal, used as reference drug, were dissolved in DMSO at a concentration of 7.2 mM providing a primary stock solution. By 5-fold dilution in DMSO of the primary stock solution the second stock solution was obtained with a final concentration of 1.44 mM. 1 mg of lyophilized wt-TTR was dissolved in 1 mL of double distilled water and 1.5 mL of 10 mM phosphate buffer (100 mM KCl, 1.7 mM EDTA) to obtain 2.5

mL of 7.2 µM TTR solution (pH 7.6). 99 µL of this TTR solution was dispensed into wells of 96-well microplate [32] and then 1 µL of the second stock solution was added. These solutions were incubated for 30 minutes at room temperature. After this period 100 µL of 200 mM acetate (pH 4.4), 100 mM KCl, 1.7 mM EDTA buffer were added in each well in order to obtain the optimal pH for the growth of fibrils and also to have a final concentration of 3.6 µM for TTR and 7.2 µM for inhibitor compound. The 96-well microplate was incubated at 37 °C for 72 h without stirring. After 72 h the solution was vortexed to redistribute any precipitate that had formed, and the optical density was measured at 400 nm using a SPECTROstarNano (200-1000 nm) UV/Vis spectrophotometer. The assays were performed in triplicate. The percentage of fibril formation was determined as previously described [33]. Prior to performing the assay, the solubility of all inhibitor compounds and the absence of any absorbance at 400 nm were checked to ensure that the turbidity depends only upon the presence of TTR amyloid fibrils.

5.4 Thioflavin T fluorescence assay

Wild-type TTR (7.2 µM), purchased from Calbiochem (EDM Millipore), was incubated for 6 hours at 37° C in 10 mM phosphate buffer (pH 7.0) with or without 10 µM EGCG (purchased from Sigma-Aldrich) and compounds **1a-e**. All samples were successively mixed with 200 mM acetate buffer (pH 4.4) and incubated at 37° C for 96 hours (final concentration of TTR 3.6 µM). After incubation, amyloid fibril formation was assessed by a Thioflavin T binding assay (10 µM ThT in 50 mM glycine buffer; TTR concentration at 0.045 µM). Amyloid fibril ratio (%) = 100 x (fluorescence TTR + compound / fluorescence without compound). Bars are representative of 11 measurements from the same experiment. Values represent the mean ± the standard error. Statistical significance was calculated by an ANOVA test (* $P < 0.05$, ** $P < 0.01$, *** $P < 0.001$, n.s. not significantly different).

5.5 Recombinant expression of TTR in E. coli

5.5.1 Design of expression plasmid

Figure 6. Graphic representation of TTR plasmid.

The plasmid expression carries a T7 promoter/terminator, a hexa-histidine (6HIS) tag for nickel affinity purification, a Tobacco Etch Virus (TEV) protease cleavage site (ENLYFQ/G) and a gene encoding the TTR. The 6HIS tag is placed between the fusion partner (DsbC) and the TEV site, Figure 6. [34]. The synthetic gene optimized for recombinant expression of TTR in *E. coli* (BL21 5DE3 pLysS strain) was ordered from Eurofins.

5.5.2 Protein expression

Expression strain BL21 (DE3) pLysS was obtained after a heat-shock transformation of competent cells with the expression plasmid. Transformed cells were used to inoculate pre-cultures containing 10 ml of LB media supplemented with ampicillin for overnight at 37°C. The following morning, a Fernbach flask containing 1L of ZYP-5052 auto-medium and ampicillin was inoculated with the overnight culture of BL21 (DE3) pLysS to reach 0.05 O.D. at 600 nm. The culture was grown in auto-induction medium ZYP-5052 supplemented with ampicillin. ZYP-5052 medium is a buffered complex medium containing glucose, lactose and glycerol formulated to induce protein expression after glucose depletion [35]. Expression was performed using a standardized two-step process. In the first part of fermentation, cells were grown at 37° C to quickly reach the glucose depletion phase just before the induction. After that step (4 hours) the temperature was lowered to 20°C for 18h to favor soluble protein expression. After 18h, cells were pelleted by centrifugation and resuspended in lysis buffer containing 100 mM Tris HCl pH 8, 150mM NaCl, 5% glycerol. 2 µl of benzonase and 0.1 M $MgCl_2$ were added to the suspension. After 30 min at 4 ° C with gentle stirring, the cells were lysed by two passes at 1.5 kbar on EMULSIFLEX. After centrifugation for 45 min at 18.000 rpm at 4°C, the soluble extract contained in the supernatant is separated from the insoluble fraction contained in the pellet.

5.5.3 Purification and TEV cleavage of DSBC-TTR

The soluble extract was filtered through 0.22 µm and loaded on a 5 ml HisTrap^{TM}FF column (GE Healthcare) with a flow rate of 1 ml/min. Buffers used for purification were binding buffer containing 100 mM tris-HCl pH 8, 150 mM NaCl, 5 mM Imidazole, 5% Glycerol and elution buffer containing 100 mM Tris-HCl pH 8, 150 mM NaCl, 500 mM imidazole, 5% Glycerol. The 6His-tagged fusion protein was eluted with a linear gradient (0 to 100% B in 30 min at a flow rate of 1 ml/min. The fractions containing the 6His-tagged fusion protein were pooled and dialyzed for 3h against buffer containing 100 mM Tris HCl pH 8, 150 mM NaCl using a Spectra/Por® Dialysis Membrane (MWCO: 3500). The protein of interest was then cleaved with 10% (w/w) TEV protease overnight at 4°C.

5.5.4 Purification of TTR

The TEV cleavage was loaded on 5 ml HisTrap^{TM}FF column (GE Healthcare) with a flow rate of 1 ml/min. The protein DSBC and TEV protease with 6His-tag were binding on the column. The TTR was recovered in the unrestrained fraction and dialyzed for 3h against buffer containing 100 mM Tris HCl pH 8, 150 mM NaCl using a Spectra/Por® Dialysis Membrane (MWCO: 3500). The last step was a purification of TTR on Size-exclusion chromatography (SEC) Sephacryl ® S-100 HR GE Healthcare in buffer 100 mM Tris HCl pH 8, 150 mM NaCl. TTR was concentrated to 5.38 mg/ml.

5.6 Crystallization experiments

Crystallization experiments were carried out with recombinant TTR. The crystallization trials were performed by sitting drop vapor diffusion Cryst ChemTM plates with 1 µl drops of protein and 1 µl drops of precipitant, stored in a constant temperature incubator at 20°C. The TTR–inhibitors crystal complexes of compounds **1c** and **1d** were prepared from TTR at 4.93 mg/ml and 10 mM of ligands dissolved in DMSO, in a volumetric ratio of 6:1, according to previously reported strategy.[27] All crystals were obtained from commercial solution #1_1.B (15% PEG 600, 0.2 M Imidazole Malate pH 5.5) of Stura Footprint Screen (Molecular Dimensions Ltd., Cambridge, UK).[31] For X-ray data collection, the crystals were cryoprotected by soaking cryoprotectant solution composed of 40% of SM1 according to the protocol previously described. [36] In order to avoid the leakage of the ligand during the flash-cooled in liquid nitrogen, the inhibitors were added to the cryoprotectant solution and soaked for 30 min at room temperature.

The data sets for the TTR-ligands crystal complexes were collected on the beamline PROXIMA 2A at Synchrotron SOLEIL storage ring in St. Aubin, France.[37] The MX data collections were carried out using micro-focused X-rays (FWHM 10 µm x 5 µm) using both helical scan and standard rotation methods.[38] Data processing was carried out using XDS with the ‘‘xdsme’’ script (https://github.com/legrandp/xdsme) to optimize data quality.

Molecular replacement was carried out using BUSTER.[39] The ligand restraint file was built using the smiles code in phenix.elbow[40] or with the monomer library sketcher from the CCP4 package.[41] The electron density maps were viewed and fitted in COOT.[42] The structures were subjected to various cycles of rebuilding and refinement with BUSTER and PHENIX.[43] The RMSD analysis was carried out using and SUPERPOSE.[44] The figures have been made with PyMOL.[45]

Acknowledgements

Diffraction data were collected on the PROXIMA 2A beamline at Synchrotron SOLEIL (Saint-Aubin, France). We are most grateful to the beamline scientists, in particular Pierre Legrand. The authors would like thank to undergraduates Matilde Casella and Matteo Poccioni (University of Pisa) for the contribution to the chemical synthesis.

This work was supported by the Italian *Ministero dell'Istruzione, dell'Universitá e della Ricerca* (PRIN 20109MXHMR_007).

References

[1] H. Brugmans, Review Articles, Gov. Oppos. 5 (1970) 107–128. https://doi.org/10.1111/j.1477-7053.1970.tb00496.x.

[2] P. Westermark, K. Sletten, B. Johansson, G.G. Cornwell, Fibril in senile systemic amyloidosis is derived from normal transthyretin., Proc. Natl. Acad. Sci. U. S. A. 87 (1990) 2843–2845. http://www.pubmedcentral.nih.gov/articlerender.fcgi?artid=53787&tool=pmcentrez&rendertype=abstract.

[3] C. Nilsson, M.G. Achen, Thyroxine transport from blood to brain via transthyretin synthesis in choroid plexus, (2019) 338–345.

[4] J. a Hamilton, M.D. Benson, Transthyretin : a review from a structural perspective, Cell. Mol. Life Sci. 58 (2001) 1491–1521. https://doi.org/doi: 10.1007/PL00000791.

[5] F. Chiti, C.M. Dobson, Protein Misfolding , Functional Amyloid , and Human Disease, (2006). https://doi.org/10.1146/annurev.biochem.75.101304.123901.

[6] A.L. Schwarzman, D. Goldgaber, Interaction of transthyretin with amyloid beta-protein: binding and inhibition of amyloid formation., Ciba Found. Symp. 199 (1996) 144–146. http://www.ncbi.nlm.nih.gov/pubmed/8915609.

[7] X. Li, X. Zhang, A.R.A. Ladiwala, D. Du, J.K. Yadav, P.M. Tessier, P.E. Wright, J.W. Kelly, J.N. Buxbaum, Mechanisms of transthyretin inhibition of $β$-amyloid aggregation in vitro., J. Neurosci. 33 (2013) 19423–19433. https://doi.org/10.1523/JNEUROSCI.2561-13.2013.

[8] T. Gi, J. Saavedra, E. Cotrina, J. Quintana, J. Llop, G. Arsequell, I. Cardoso, Undiscovered Roles for Transthyretin : From a Transporter Protein to a New Therapeutic Target for Alzheimer ' s Disease, (n.d.).

[9] M.A. Lovell, J.D. Robertson, W.J. Teesdale, J.L. Campbell, W.R. Markesbery, Copper, iron and zinc in Alzheimer's disease senile plaques., J. Neurol. Sci. 158 (1998) 47–52. https://doi.org/10.1016/S0022-510X(98)00092-6.

[10] S.S. Leal, H.M. Botelho, C.M. Gomes, Metal ions as modulators of protein conformation and misfolding in neurodegeneration, Coord. Chem. Rev. 256 (2012) 2253–2270. https://doi.org/10.1016/j.ccr.2012.04.004.

[11] L. Ciccone, C. Policar, E.A. Stura, W. Shepard, Human TTR conformation altered by rhenium tris-carbonyl derivatives., J. Struct. Biol. 195 (2016) 353–364. https://doi.org/10.1016/j.jsb.2016.07.002.

[12] L. Ciccone, C. Fruchart-gaillard, G. Mourier, M. Savko, S. Nencetti, E. Orlandini, D. Servent, E.A. Stura, W. Shepard, Copper mediated amyloid- β binding to Transthyretin, Sci. Rep. (2018) 1–11. https://doi.org/10.1038/s41598-018-31808-5.

[13] A. Wojtczak, V. Cody, J.R. Luft, W. Pangborn, Structures of Human Transthyretin Complexed with Thyroxine at 2.0 ÅResolution and 3',5'-Dinitro- N -acetyl- L -thyronine at 2.2 ÅResolution, Acta Crystallogr. Sect. D Biol. Crystallogr. 52 (1996) 758–765. https://doi.org/10.1107/S0907444996003046.

[14] J.W. Kelly, Alternative conformations of amyloidogenic proteins govern their behavior, (1996).

[15] J.W. Kelly, Amyloid fibril formation and protein misassembly: a structural quest for insights into amyloid and prion diseases., Structure. 5 (1997) 595–600. http://www.ncbi.nlm.nih.gov/pubmed/9195890.

[16] P. Hammarström, R.L. Wiseman, E.T. Powers, J.W. Kelly, Prevention of transthyretin amyloid disease by changing protein misfolding energetics., Science. 299 (2003) 713–716. https://doi.org/10.1126/science.1079589.

[17] S.M. Johnson, R.L. Wiseman, Y. Sekijima, N.S. Green, S.L. Adamski-werner, J.W. Kelly, Native State Kinetic Stabilization as a Strategy To Ameliorate Protein Misfolding Diseases : A Focus on the Transthyretin Amyloidoses Introduction to the Transthyretin Amyloidoses, 38 (2005) 911–921. https://doi.org/10.1021/ar020073i.

[18] J. Herbert, J.N. Wilcox, K.-T.C. Pham, R.T. Fremeau, M. Zeviani, A. Dwork, D.R. Soprano, A. Makover, D.S. Goodman, E.A. Zimmerman, J.L. Roberts, E.A. Schon, Transthyretin, Neurology. 36 (1986) 900 LP – 900. https://doi.org/10.1212/WNL.36.7.900.

[19] S. Nencetti, A. Rossello, E. Orlandini, Tafamidis (Vyndaqel): A light for FAP patients, ChemMedChem. 8 (2013) 1617–1619. https://doi.org/10.1002/cmdc.201300245.

[20] C.E. Bulawa, S. Connelly, M. DeVit, L. Wang, C. Weigel, J. a. Fleming, J. Packman, E.T. Powers, R.L. Wiseman, T.R. Foss, I. a. Wilson, J.W. Kelly, R. Labaudiniere, Tafamidis, a potent and selective transthyretin kinetic stabilizer that inhibits the amyloid cascade, Proc. Natl. Acad. Sci. 109 (2012) 9629–9634. https://doi.org/10.1073/pnas.1121005109.

[21] M.S. Maurer, J.H. Schwartz, B. Gundapaneni, P.M. Elliott, G. Merlini, M. Waddington-Cruz, A. V. Kristen, M. Grogan, R. Witteles, T. Damy, B.M. Drachman, S.J. Shah, M. Hanna, D.P. Judge, A.I. Barsdorf, P. Huber, T.A. Patterson, S. Riley, J. Schumacher, M. Stewart, M.B. Sultan, C. Rapezzi, Tafamidis treatment for patients with transthyretin amyloid cardiomyopathy, N. Engl. J. Med. 379 (2018) 1007–1016. https://doi.org/10.1056/NEJMoa1805689.

[22] S. Nencetti, E. Orlandini, TTR fibril formation inhibitors: is there a SAR?, Curr. Med. Chem. 19 (2012) 2356–2379. https://doi.org/10.2174/092986712800269326.

[23] S.K. Palaninathan, N.N. Mohamedmohaideen, E. Orlandini, G. Ortore, S. Nencetti, A. Lapucci, A. Rossello, J.S. Freundlich, J.C. Sacchettini, Novel Transthyretin Amyloid Fibril Formation Inhibitors: Synthesis, Biological Evaluation, and X-Ray Structural Analysis, PLoS One. 4 (2009) e6290. https://doi.org/10.1371/journal.pone.0006290.

[24] L. Ciccone, S. Nencetti, A. Rossello, L. Tepshi, E. a Stura, E. Orlandini, X-ray crystal structure and activity of fluorenyl-based compounds as transthyretin fibrillogenesis inhibitors., J. Enzyme Inhib. Med. Chem. 6366 (2015) 1–10. https://doi.org/10.3109/14756366.2015.1070265.

[25] L. Ciccone, S. Nencetti, A. Rossello, E.A. Stura, E. Orlandini, Synthesis and structural analysis of halogen substituted fibril formation inhibitors of Human Transthyretin (TTR)., J. Enzyme Inhib. Med. Chem. 31 (2016) 40–51. https://doi.org/10.3109/14756366.2016.1167048.

[26] N. Ferreira, N.P. Gonçalves, M.J. Saraiva, M.R. Almeida, Curcumin: A multi-target disease-modifying agent for late-stage transthyretin amyloidosis, Sci. Rep. 6 (2016) 26623. https://doi.org/10.1038/srep26623.

[27] L. Ciccone, L. Tepshi, S. Nencetti, E.A. Stura, Transthyretin complexes with curcumin and bromo-estradiol: evaluation of solubilizing multicomponent mixtures., N. Biotechnol. 32 (2015) 54–64. https://doi.org/10.1016/j.nbt.2014.09.002.

[28] P. Florio, C. Folli, M. Cianci, D. Del Rio, G. Zanotti, R. Berni, Transthyretin binding heterogeneity and antiamyloidogenic activity of natural polyphenols and their metabolites, J. Biol. Chem. 290 (2015) 29769–29780. https://doi.org/10.1074/jbc.M115.690172.

[29] M. Miyata, T. Sato, M. Kugimiya, M. Sho, T. Nakamura, S. Ikemizu, M. Chirifu, M. Mizuguchi, Y. Nabeshima, Y. Suwa, H. Morioka, T. Arimori, M.A. Suico, T. Shuto, Y. Sako, M. Momohara, T. Koga, S. Morino-Koga, Y. Yamagata, H. Kai, The crystal structure of the green tea polyphenol (-)-epigallocatechin gallate-transthyretin complex reveals a novel binding site distinct from the thyroxine binding site., Biochemistry. 49 (2010) 6104–6114. https://doi.org/10.1021/bi1004409.

[30] L. Ciccone, N. Tonali, E. Orlandini, S. Nencetti, E. Orlandini, Natural compounds as inhibitors of Transthyretin amyloidosis and neuroprotective agents: analysis of structural data for future drug design, J. Enzyme Inhib. Med. Chem. (2020). https://doi.org/10.1080/14756366.2020.1760262.

[31] E.A. Stura, G.R. Nemerow, I.A. Wilson, Strategies in the crystallization of glycoproteins and protein complexes, J. Cryst. Growth. 122 (1992) 273–285. https://doi.org/10.1016/0022-0248(92)90256-I.

[32] I. Dolado, J. Nieto, M.J.M. Saraiva, G. Arsequell, G. Valencia, A. Planas, Kinetic assay for high-throughput screening of in vitro transthyretin amyloid fibrillogenesis inhibitors., J. Comb. Chem. 7 (2005) 246–252. https://doi.org/10.1021/cc049849s.

[33] V.B. Oza, C. Smith, P. Raman, E.K. Koepf, H.A. Lashuel, H.M. Petrassi, K.P. Chiang, E.T. Powers, J. Sachettinni, J.W. Kelly, Synthesis, structure, and activity of diclofenac analogues as transthyretin amyloid fibril formation inhibitors., J. Med. Chem. 45 (2002) 321–332. https://doi.org/10.1021/jm010257n.

[34] H. Nozach, C. Fruchart-Gaillard, F. Fenaille, F. Beau, O.H.P. Ramos, B. Douzi, N.J. Saez, M. Moutiez, D. Servent, M. Gondry, R. Thaï, P. Cuniasse, R. Vincentelli, V. Dive, High throughput screening identifies disulfide isomerase DsbC as a very efficient partner for recombinant expression of small disulfide-rich proteins in E. coli, Microb. Cell Fact. 12 (2013) 1–16. https://doi.org/10.1186/1475-2859-12-37.

[35] F.W. Studier, Protein production by auto-induction in high density shaking cultures., Protein Expr. Purif. 41 (2005) 207–234. http://www.ncbi.nlm.nih.gov/pubmed/15915565.

[36] E.A. Stura, L. Ciccone, L. Tepshi, L. Vera, L. Tepshi, E.A. Stura, Multicomponent mixtures for ligand solubilization and cryoprotection, in: ECM 2015, 2015: p. 2015.

[37] D. Duran, S. Le Couster, K. Desjardins, a Delmotte, G. Fox, R. Meijers, T. Moreno, M. Savko, W. Shepard, PROXIMA 2A – A New Fully Tunable Micro-focus Beamline for Macromolecular Crystallography, J. Phys. Conf. Ser. 425 (2013) 12005. https://doi.org/10.1088/1742-6596/425/1/012005.

[38] I. Polsinelli, M. Savko, C. Rouanet-Mehouas, L. Ciccone, S. Nencetti, E. Orlandini, E.A. Stura, W. Shepard, Comparison of helical scan and standard rotation methods in single-crystal X-ray data collection strategies., J. Synchrotron Radiat. 24 (2017) 42–52. https://doi.org/10.1107/S1600577516018488.

[39] O.S. Smart, O. Thomas, C. Flensburg, W. Paciorek, A. Sharff, research papers Exploiting structure similarity in refinement : automated NCS and target-structure restraints in BUSTER, (2012) 368–380. https://doi.org/10.1107/S0907444911056058.

[40] N.W. Moriarty, R.W. Grosse-Kunstleve, P.D. Adams, electronic Ligand Builder and Optimization Workbench (eLBOW): a tool for ligand coordinate and restraint generation., Acta Crystallogr. D. Biol. Crystallogr. 65 (2009) 1074–1080. https://doi.org/10.1107/S0907444909029436.

[41] M.D. Winn, C.C. Ballard, K.D. Cowtan, E.J. Dodson, P. Emsley, P.R. Evans, R.M. Keegan, E.B. Krissinel, A.G.W. Leslie, A. McCoy, S.J. McNicholas, G.N. Murshudov, N.S. Pannu, E.A. Potterton, H.R. Powell, R.J. Read, A. Vagin, K.S. Wilson, Overview of the CCP4 suite and current developments., Acta Crystallogr. D. Biol. Crystallogr. 67 (2011) 235–242. https://doi.org/10.1107/S0907444910045749.

[42] P. Emsley, B. Lohkamp, W.G. Scott, K. Cowtan, Features and development of Coot., Acta Crystallogr. D. Biol. Crystallogr. 66 (2010) 486–501. https://doi.org/10.1107/S0907444910007493.

[43] P.D. Adams, P. V. Afonine, G. Bunkóczi, V.B. Chen, I.W. Davis, N. Echols, J.J. Headd, L.-W.W. Hung, G.J. Kapral, R.W. Grosse-Kunstleve, A.J. McCoy, N.W. Moriarty, R. Oeffner, R.J. Read, D.C. Richardson, J.S. Richardson, T.C. Terwilliger, P.H. Zwart, PHENIX: a comprehensive Python-based system for macromolecular structure solution., Acta Crystallogr. D. Biol. Crystallogr. 66 (2010) 213–221. https://doi.org/10.1107/S0907444909052925.

[44] E. Krissinel, K. Henrick, Secondary-structure matching (SSM), a new tool for fast protein structure alignment in three dimensions., Acta Crystallogr. D. Biol. Crystallogr. 60 (2004) 2256–2268. https://doi.org/10.1107/S0907444904026460.

[45] W.L. DeLano, The PyMOL Molecular Graphics System, in: L. Schrödinger, New York Editor, 2010.